1521-009X/49/12/1100–1108$35.00
DRUG METABOLISM AND DISPOSITION

https://doi.org/10.1124/dmd.121.000554
Drug Metab Dispos 49:1100–1108, December 2021

Complex Cytochrome P450 Kinetics Due to Multisubstrate Binding and Sequential Metabolism. Part 2. Modeling of Experimental Data[S]

Erickson M. Paragas,[1] Zeyuan Wang,[1] Ken Korzekwa, and Swati Nagar

Department of Pharmaceutical Sciences, Temple University School of Pharmacy, Philadelphia, Pennsylvania

Received May 25, 2021; accepted August 30, 2021

ABSTRACT

Three CYP3A4 substrates, midazolam, ticlopidine, and diazepam, display non–Michaelis-Menten kinetics, form multiple primary metabolites, and are sequentially metabolized to secondary metabolites. We generated saturation curves for these compounds and analyzed the resulting datasets using a number of single-substrate and multisubstrate binding models. These models were parameterized using rate equations and numerical solutions of the ordinary differential equations. Multisubstrate binding models provided results superior to single-substrate models, and simultaneous modeling of multiple metabolites provided better results than fitting the individual datasets independently. Although midazolam datasets could be represented using standard two-substrate models, more complex models that include explicit enzyme-product complexes were needed to model the datasets for ticlopidine and diazepam. In vivo clearance predictions improved markedly with the use of in vitro parameters from the complex models versus the Michaelis-Menten equation. The results highlight the need to use sufficiently complex kinetic schemes instead of the Michaelis-Menten equation to generate accurate kinetic parameters.

SIGNIFICANCE STATEMENT

The metabolism of midazolam, ticlopidine, and diazepam by CYP3A4 results in multiple metabolites and sequential metabolism. This study evaluates the use of rate equations and numerical methods to characterize the in vitro enzyme kinetics. Use of complex cytochrome P450 kinetic models is necessary to obtain accurate parameter estimates for predicting in vivo disposition.

Introduction

In vitro P450-mediated metabolism assays are used to predict in vivo compound stability and potential for drug-drug interactions (Zhang and Wong, 2005; Vieira et al., 2014; Di, 2017; Yadav et al., 2020). However, interpreting experimental in vitro data can be difficult because of complex P450 enzymology. The need to metabolize a very large number of xenobiotics results in unusual kinetics with respect to ligand selectivity (Ekroos and Sjögren, 2006). X-ray crystallography studies confirm that many P450s have large and flexible active sites that can simultaneously bind multiple substrates (Li and Poulos, 2004; Nguyen et al., 2016; Sevrioukova and Poulos, 2017). This can result in non–Michaelis-Menten (MM) or atypical kinetics, which do not display standard hyperbolic saturation curves (Korzekwa et al., 1998; Cameron et al., 2005; Kapelyukh et al., 2008; Schoch et al., 2008; Shah et al., 2012). Thus, the estimation of in vitro kinetic parameters (V_{max}, K_m, and V_{max}/K_m using MM approaches for compounds that display atypical kinetics (see part 1) may lead to overestimation or underestimation, especially with sigmoidal kinetics. The production of multiple metabolites adds to the complexities in estimation of these in vitro parameters (Wienkers and Rock, 2014). For example, for compounds that follow MM kinetics, the product ratios are constant at different substrate concentrations, whereas this ratio may not be constant for compounds that exhibit atypical kinetics (see part 1).

Moreover, in addition to the pharmacological effect of the parent drug, its oxidative metabolites may exhibit some efficacy at the intended biologic target (Garattini, 1985; Caccia and Garattini, 1990; Obach, 2013). For example, norketamine, the active metabolite of ketamine, may contribute equally to the pharmacological effect (Hijazi and Boulieu, 2002). The topoisomerase 1 inhibitor irinotecan is a prodrug that undergoes the hydrolysis to form SN-38, which exhibits over 1000 times more potency (Kawato et al., 1991). The primary metabolites from drugs like ticlopidine (Yoneda et al., 2004; Farid et al., 2010) and diazepam (Rouini et al., 2008) are further metabolized by P450s to form the pharmacologically active metabolites. These examples highlight the importance of sequential metabolism. To our knowledge, no standard rate equations are available to characterize sequential metabolism.

In part 1, we showed that numerical method analysis of the non-MM kinetics provided a more accurate and precise estimation of in vitro kinetic parameters. When used for enzyme kinetics, the numerical approach does not rely on steady-state assumptions or initial-rate conditions and can model mechanistic complexities of P450 kinetics, including multiple-substrate binding and sequential metabolism. In part 2, we use numerical methods to characterize the in vitro metabolism of midazolam, ticlopidine, and diazepam. The standard rate equations and ordinary differential equation (ODE) models

This work was supported by National Institutes of Health National Institute of General Medical Sciences [Grants R01GM104178 and R01GM114369].

None of the authors have any financial disclosures or any conflicts of interest.

[1]E.M.P. and Z.W. contributed equally to the work.

https://dx.doi.org/10.1124/dmd.121.000554.

[S] This article has supplemental material available at dmd.aspetjournals.org.

ABBREVIATIONS: AICc, corrected Akaike information criteria; DZP, diazepam; EH, Eadie-Hofstee; EP, entrance potential; ES, enzyme-substrate complex (single-substrate binding); ESS, enzyme-substrate-substrate complex (two-substrate binding); k_{cat}, catalytic rate constant; K_m, Michaelis-Menten constant; MDZ, midazolam; MM, Michaelis-Menten; NDP, nordiazepam; ODE, ordinary differential equation; 1′-OH-MDZ, 1′-hydroxymidazolam; 4-OH-MDZ, 4-hydroxymidazolam; OXP, oxazepam; P450, cytochrome P450; TCP, ticlopidine; TZP, temazepam; V_{max}, maximal velocity.

describing single- and two-substrate binding kinetics were fit to midazolam, ticlopidine, and diazepam saturation experiments. For each dataset, various kinetic schemes were evaluated and compared.

Materials and Methods

Ticlopidine hydrochloride (TCP), midazolam (MDZ), 4-hydroxymidazolam, diazepam (DZP), nordiazepam (NDP), temazepam (TZP), oxazepam (OXP), and temazepam-d5 (TZP-d5) were purchased from Sigma-Aldrich (St. Louis, MO), and 1′-hydroxymidazolam was purchased from Cayman Chemical (Ann Arbor, MI). Recombinant human CYP3A4 supersomes and NADPH-regenerating system were purchased from Corning (Woburn, MA). The 2-oxo-TCP, and TCP *N*-oxide were purchased from Toronto Research Chemicals (Toronto, CA). The monobasic potassium phosphate, dibasic potassium phosphate, and EDTA used for the potassium phosphate buffer were purchased from JT Baker (Center Valley, PA). Phenacetin was a gift from the laboratory of Jeffrey P. Jones (Washington State University).

CYP3A4 in vitro incubations: The CYP3A4-mediated metabolism (Fig. 1) of three substrates, MDZ, TCP, and DZP, was evaluated. Substrate concentrations were: 0.39–400 μM MDZ or 2.34–300 μM TCP in 100 mM potassium phosphate buffer (pH 7.4) containing 0.1 mM EDTA or 2.5–400 μM DZP in 0.5% v/v methanol and buffer. Each substrate was preincubated with the recombinant human CYP3A4 supersomes (0.0025 μM for MDZ, 0.005 μM for TCP, and 0.01 μM for DZP) for 2.0 minutes (MDZ and TCP) or 5.0 minutes (DZP) to attain 37°C. Reaction was started with the addition of NADPH. The NADPH-regenerating system was 1.3 mM $NADP^+$, 3.3 mM glucose-6-phosphate, 0.4 U/ml glucose-6-phosphate dehydrogenase, and 3.3 mM magnesium chloride. All incubations were allowed to proceed at 37°C for 5.0 minutes for MDZ and TCP and 3.0 minutes for DZP. The final reaction volume was 100 μl. The reaction was quenched by the addition of 100 μl of acetonitrile containing internal standard (phenacetin for MDZ and TCP and temazepam-d5 for DZP). All samples were then centrifuged at 10,000 ×*g* for 10 minutes (2,200 ×*g* for 60 minutes for DZP incubations), and the supernatant was collected for liquid chromatography–tandem mass spectrometry analysis. In addition to incubations with DZP as the substrate, separate incubations were performed to evaluate OXP formation from either TZP or NDP. For these incubations, all conditions were the same as the DZP incubations above.

Samples were analyzed using an Agilent 1100 series high-performance liquid chromatography system (Agilent Technologies, Santa Clara, CA). Mobile phase A consisted of 0.1% (v/v) formic acid in water, and mobile phase B comprised 0.1% formic acid (v/v) in acetonitrile. For MDZ and TCP metabolites, the chromatography was performed on a Zorbax Eclipse XDB-C8 (4.6 × 150 mm, 5 microns) column equipped with a C18 guard column (4 × 2 mm) (Phenomenex, Torrance, CA). The initial conditions were 30% mobile phase B for 0.5 minutes at 800 μl/min. Chromatographic separation was performed using a linear gradient over 6 minutes to 100% mobile phase B. Mobile phase B was then held constant for 0.5 minutes, and this was followed by a linear gradient back to 30% mobile phase B over 0.1 minutes. Finally, the column was re-equilibrated to the initial conditions over 3 minutes. The total chromatographic assay time is 9 minutes per sample.

TABLE 1

Mass spectrometer parameters for substrates and metabolites

Compound	CE	DP	EP	CXP	MRM
1′-Hydroxymidazolam	35	70	10	15	342.2 → 324.1
4-Hydroxymidazolam	35	70	10	15	342.2 → 234.0
2-Oxo-ticlopidine	15	70	10	15	280.2 → 125.1
Ticlopidine *N*-oxide	15	70	10	15	280.2 → 235.0
Diazepam	38	55	10	10	285.1 → 192.8
Temazepam	15	50	10	15	301.1 → 254.8
Nordiazepam	30	50	10	15	271.1 → 139.8
Oxazepam	30	50	10	15	287.1 → 240.9
Phenacetin (IS)	30	70	10	15	180.2 → 110.1
Temazepam-d5 (IS)	32	55	10	18	306.1 → 259.8

CE, collision energy; CXP, collision exit potential; DP, declustering potential; IS, internal standard; MRM, multiple reaction monitoring

For DZP metabolites, the chromatography was performed on a Luna 3 μm C18(2), 50 × 2-mm column (Phenomenex, Torrance, CA) equipped with C18 guard column (4 × 2.0 mm). The initial conditions were 10% mobile phase B for 0.5 minutes at 400 μl/min. Chromatographic separation was performed using a linear gradient over 1 minute to 95% mobile phase B. Mobile phase B was then held constant for 2 minutes, followed by a linear gradient back to 10% mobile phase B over 0.5 minutes. The column was re-equilibrated to the initial conditions over 3.5 minutes. The total chromatographic assay time is 7.5 minutes per sample.

The quantitation of all metabolites was conducted on an API 4000 Q-Trap mass spectrometry system (Applied Biosystems/MDS Sciex, Foster City, CA) with turbospray ESI operating in positive ion mode. The analytes were detected by multiple reaction monitoring mode using ions and mass spectrometer tune parameters in Table 1.

The standard rate equations and ODEs describing two-substrate binding kinetics were used (Fig. 2) to fit the model to the metabolite formation datasets. For enzyme-substrate-multiple product formation (ESP1P2 for single substrate binding, and ESSP1P2 for multisubstrate binding) modeling, all metabolite data were used simultaneously for model fitting. All association rate constants were fixed at 270 $\mu M^{-1}min^{-1}$. Therefore, dissociation rate constants define enzyme affinities (Barnaba et al., 2016; Yadav et al., 2018). Eadie-Hofstee (EH) and product ratio plots were also used to analyze the in vitro data sets.

The shape of EH plots of the raw data were used to initially diagnose sigmoidal, biphasic, or substrate inhibition. For biphasic kinetics, an initial estimate of K_{m1}, K_{m2}, k_{cat1}, and k_{cat2} can be obtained from the EH plot (see Supplemental Fig. 1). K_{m1} and K_{m2} can be estimated from the slope of the line through the highest velocity/[substrate] data points: L1 and the lowest velocity/[substrate] data points

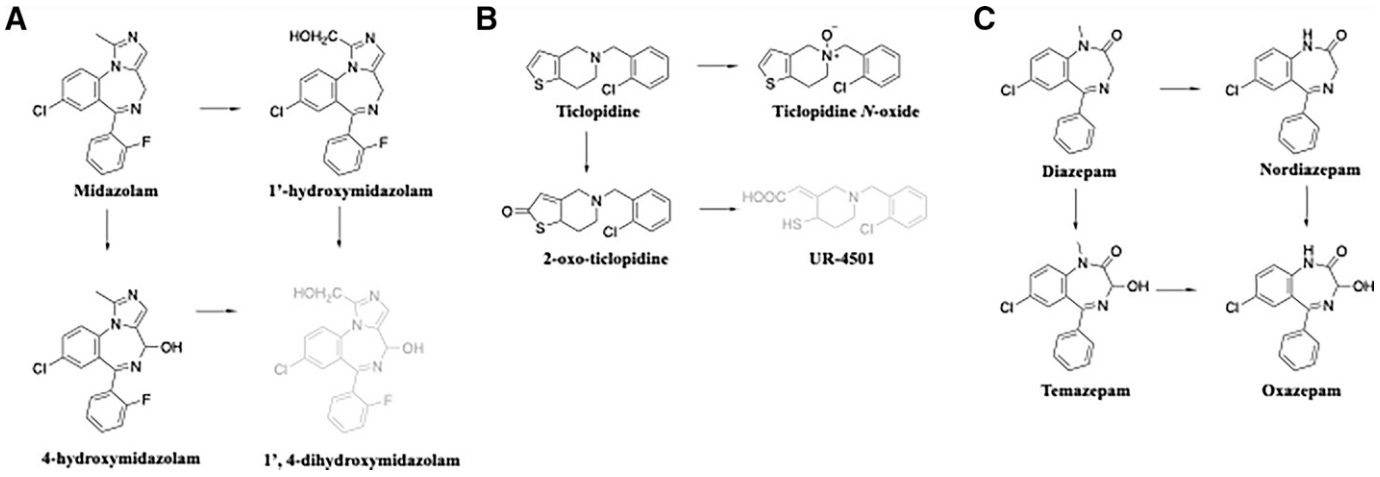

Fig. 1. Substrate metabolism via CYP3A. (A) Midazolam metabolism. (B) Ticlopidine metabolism. (C) Diazepam metabolism. Metabolites that are reported in the literature but were not analyzed in the present study because of lack of authentic available standards are in light gray.

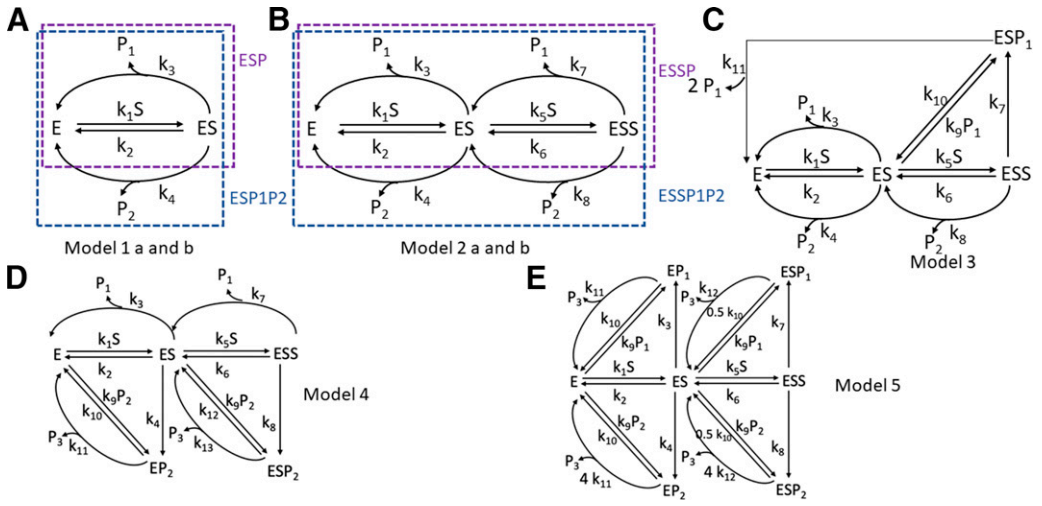

Fig. 2. (A) Model 1 with single (ES)-binding kinetic models for single (model 1a)- or multiple-product (model 1b) formation. (B) Model 2 two-substrate (ESS) binding kinetic models for single (model 2a)- or multiple-product (model 2b) formation. (C) Model 3, a sequential metabolism model for ESS kinetics with slow product release. (D) Model 4, a sequential metabolism model with complex formation between E and P2. (E) Model 5, a sequential metabolism model with complex formation between E and P1, and E and P2.

and L2, respectively. Parameters k_{cat1} and k_{cat2} can be estimated from the intersection points between L1 and *y*-axis and L2 and *y*-axis, respectively. For substrate inhibition, initial estimates of parameters except K_{m2} can be obtained with EH plots (see Supplemental Fig. 1). It is difficult to estimate the kinetic parameters for sigmoidal kinetics. As mentioned in part 1, sigmoidal kinetics can be accounted for by several different cases. An initial estimate of k_{cat2} can be obtained directly from the saturation curves if high enough concentration of substrate were used.

Mathematica 12.0 (Wolfram Research, Champaign, IL) was used for model fitting and plot generation. The ODEs were numerically solved with NDSolve to provide interpolated functions of each enzyme species. NonlinearModelFit function was used to parameterize the rate constants with 1/Y weighting. Specific properties, including MaxSteps → 100,000 and PrecisionGoal → infinity(∞) for NDSolve, were assigned. If necessary, finite difference derivatives were used. The corrected Akaike information criteria (AICc) was used to select the most appropriate model when comparing several models for the same dataset (Akaike, 1974). Based on saturation curves, the ability for a model to simultaneously model multiple metabolites, and product ratio curves, additional models were constructed and explored.

In vitro clearance estimates obtained from the enzyme kinetic models were scaled to predict human in vivo clearance for two compounds with known fraction metabolized by CYP3A4—MDZ and DZP. Scaling was conducted assuming a well stirred liver model and standard scaling factors scaling from microsome to liver (Obach, 2011).

Results

For all substrates, single-substrate models (model 1) were compared with two-substrate models since the industry standard is to use MM kinetics. In all cases, two-substrate models were necessary to reproduce the observed kinetics as determined by residuals and AICc values (see Supplemental Table 1). Therefore, only two-substrate model results are provided.

CYP3A4 metabolism of MDZ was monitored for the formation of 1′-OH-MDZ and 4-OH-MDZ (Fig. 3). Initial inspection of the saturation data and the EH plots for the formation of 1′-OH-MDZ and 4-OH-MDZ showed substrate inhibition and biphasic kinetics, respectively (Figs. 3A and B). Metabolism of MDZ by human CYP3A4 has been previously reported to exhibit substrate inhibition (Nguyen et al., 2016), and the metabolite ratio plot at different concentrations of MDZ supports the need for two-substrate binding models (Fig. 3C). The results for the two-substrate models (model 2) are shown in Table 2. Models for the two metabolites were parameterized individually for each metabolite (model 2a) and simultaneously (model 2b, for ODE models only).

To converge to a model with meaningful parameter standard errors, K_{m2} had to be fixed for model 2a. However, the K_{m1} values for P1 and P2 formation were not identical, which is not consistent with model 2. When P1 and P2 were modeled simultaneously, all parameters for model 2b could be optimized and resulted in meaningful and consistent parameter estimates. Also, the observed [P1]/[P2] ratio as a function of [S] was well predicted by model 2b (Fig. 3C).

TCP undergoes sequential metabolism to form the pharmacologically active metabolite UR-4501(Yoneda et al., 2004; Farid et al., 2010). For this study, only the primary metabolites were monitored because of the lack of availability of UR-4501. Many models were parameterized, and the results are given in Tables 3 and 4 and Fig. 4. The saturation and EH plots for 2-oxo-TCP showed sigmoidal saturation, and the formation of TCP *N*-oxide is biphasic (Fig. 4). Using the rate equation for model 2a, meaningful parameter estimates for K_{m2} for P2 could not be obtained even after fixing K_{m1}. This was resolved when the ODEs were used. However, the K_{m2} values for P1 (56 μM) and P2 (835 μM) were inconsistent with model 2. Model 2b was able to provide acceptable fits to the data for 2-oxo-TCP and TCP *N*-oxide, but the ratio plot was not correctly modeled (Fig. 4C). Therefore, we explored additional models, and the best fit (Fig. 4 and Table 4) was obtained with the scheme shown in Fig. 2C (model 3). This model includes an explicit ESP1 complex. This was included since P1 is ultimately converted to P3. However, in the absence of P3 data, the amount of P3 formed from ESP1 could not be defined. Any branching ratio (P1 to P3) gave identical fits. Therefore, the simplest model (no P3 formation) is reported in Fig. 4 and Table 4. Model 3 reproduces P1 and P2 formation (see EH insets, Fig. 4) and the P1/P2 ratios (Fig. 4C).

Formation of TZP and NDP from DZP shows sigmoidal kinetics (Fig. 5), with higher sigmoidicity seen for TZP formation. Similar saturation curves have been reported previously for diazepam metabolism (He et al., 2003). Fitting the standard two-substrate model (model 2a) to the individual metabolite data resulted in high parameter errors (Table 5). This is expected because of the high covariance between K_{m1}, K_{m2}, k_{cat1}, and k_{cat2} for sigmoidal models. In contrast to MDZ and TCP for which one metabolite shows substrate inhibition and biphasic kinetics, respectively, DZP metabolites both show sigmoidal kinetics. Therefore, very low k_{cat1} values are possible and could be a concern when predicting clearance (see part 1). Fitting model 2a to the individual datasets with $k_{cat1} = 0$ resulted in poorer fits with AICc values −68.9 and −149.8 compared with −78.9 and −155.7 for TZP and NDP, respectively. Fitting model 2b to the

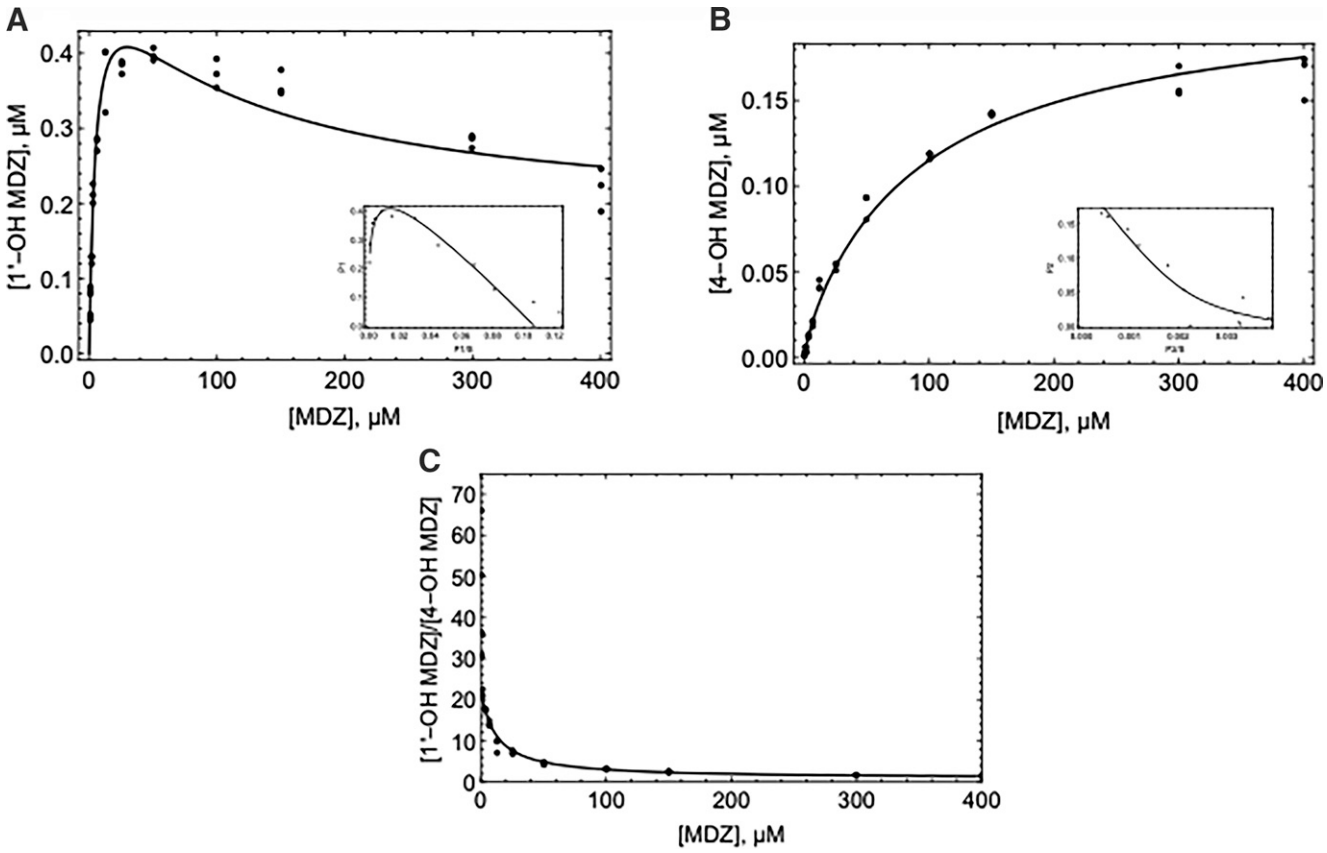

Fig. 3. Kinetic plots of midazolam metabolism by CYP3A4 (n = 3) for the formation of (A) 1′-hydroxymidazolam and (B) 4-hydroxymidazolam and (C) ratio of 1′-hydroxymidazolam to 4-hydroxymidazolam. Insets represent EH plots with mean data. Solid lines represent the fit with model 2b.

combined P1 and P2 dataset resulted in much lower parameter errors. K_m, k_{cat}, and K_m/k_{cat} values are similar to those for model 2a.

Since oxazepam (P3) is available and was quantitated in the DZP incubations, we attempted to fit several sequential models to the combined P1, P2, and P3 datasets. Simple models with rapid release of P1 and P2 (e.g., Fig. 10, A and B in part 1) failed to adequately model the data. We therefore evaluated models that include enzyme-product complexes (e.g., models 4 and 5 in Fig. 2). Using the combined P1, P2, and P3 dataset, models

TABLE 2

Scheme and kinetic parameters for midazolam metabolism with a two-substrate model
Parameters are bolded for the final "best-fit" scheme selected.

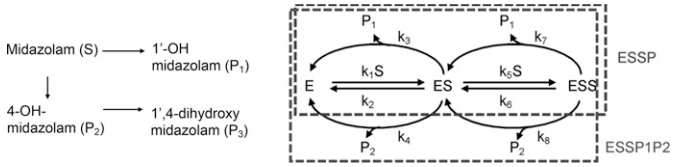

Kinetic Parameters	ESS Rate Equation	ESSP ODE	ESSP1P2 ODE
	1′-OH-MDZ		**1′-OH-MDZ**
K_{m1} (μM) = $(k_2+k_3+k_4)/k_1$	5.0 (0.4)	4.7 (0.4)	**4.8 (0.4)**
$k_{cat1}(min^{-1}) = k_3$	43.4 (1.7)	43.1 (1.7)	**43.3 (1.6)**
k_{cat1}/K_{m1} ($ml\ min^{-1}nmol^{-1}$)	8.8 (0.8)	9.2 (0.9)	**9.1 (0.8)**
K_{m2} (μM)= $(k_6+k_7+k_8)/k_5$	100 (fixed)	100 (fixed)	**103 (18)**
$k_{cat2}(min^{-1}) = k_7$	14.2 (1.2)	14.3 (1.2)	**14.1 (1.0)**
AICc	−164.3	−163.3	
	4-OH-MDZ		**4-OH-MDZ**
K_{m1} (μM) = $(k_2+k_3+k_4)/k_1$	19 (5)	19 (5)	**4.8 (0.4)**
$k_{cat1}(min^{-1}) = k_4$	5.5 (1.2)	5.5 (1.2)	**1.92 (0.26)**
k_{cat1}/K_{m1} ($ml\ min^{-1}nmol^{-1}$)	0.29 (0.10)	0.29 (0.10)	**0.40 (0.06)**
K_{m2} (μM) $(k_6+k_7+k_8)/k_5$	100 (fixed)	100 (fixed)	**103 (18)**
$k_{cat2}(min^{-1}) = k_8$	15.5 (0.5)	15.5 (0.6)	**17.2 (1.0)**
AICc	−300.1	−300.1	

ESSP, enzyme-substrate-substrate complex scheme with single product formation; ESSP1P2, enzyme-substrate-substrate complex scheme with two products formed.

TABLE 3

Scheme and kinetic parameters for ticlopidine metabolism with a two-substrate model

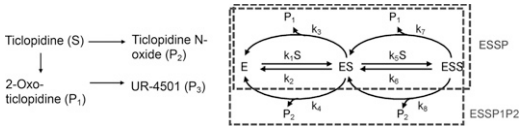

Kinetic Parameters	ESS Rate Equation	ESSP ODE	ESSP1P2 ODE
	2-Oxo-TCP		**2-Oxo-TCP**
K_{m1} (μM) = $(k_2+k_3+k_4)/k_1$	38.9 (fixed)	38.9 (fixed)	38.9 (fixed)
k_{cat1} (min^{-1}) = k_3	2.6 (0.6)	2.6 (0.6)	3.6 (0.5)
k_{cat1}/K_{m1} ($ml\ min^{-1}nmol^{-1}$)	0.066 (fixed)	0.066 (fixed)	0.093 (fixed)
K_{m2} (μM)= $(k_6+k_7+k_8)/k_5$	56 (16)	56. (16)	124 (46)
k_{cat2} (min^{-1}) = k_7	8.4 (0.5)	8.4 (0.9)	9.8 (1.0)
AICc	−175.7	−175.7	
	TCP *N*-Oxide		**TCP *N*-Oxide**
K_{m1} (μM) = $(k_2+k_3+k_4)/k_1$	38.9 (fixed)	38.9 (fixed)	38.9 (fixed)
k_{cat1} (min^{-1}) = k_4	3.1 (0.5)	3.09 (0.32)	2.3 (0.5)
k_{cat1}/K_{m1} ($ml\ min^{-1}nmol^{-1}$)	0.080 (fixed)	0.072 (fixed)	0.059 (fixed)
K_{m2} (μM) $(k_6+k_7+k_8)/k_5$	1000 (2200)[a]	835 (108)	124 (46)
k_{cat2} (min^{-1}) = k_8	21 (32)[a]	18.8 (3.2)	9.6 (1.0)
AICc	−162.4	−162.4	−331.2

ESSP, enzyme-substrate-substrate complex scheme with single product formation; ESSP1P2, enzyme-substrate-substrate complex scheme with two products formed.
[a]Parameter estimation is not valid as indicated by the high errors.

with P3 formation from varying combinations of EP1, EP2, ESP1, and ESP2 fit the data equally well (unpublished data). The one constraint across all models tested was that P3 formation was greater from P2 than from P1. The fitted parameters for simplest of these models (model 4) is shown in Table 6. For this model, K_{m1} was fixed to the value for model 2b. It was also necessary to optimize and fix K_{m3} as well.

The availability of data for the conversion of TZP and NDP to OXP (see Supplemental Fig. 2) allowed us to characterize the relative formation of P3 from P2 versus P1. For formation of OXP from both TZP and NDP, sigmoidal kinetics are observed. It was again necessary to fix K_{m2}, but varying K_{m2} between 4 and 450 μM gave relatively constant k_{cat1}/K_{m1} values of approximately 4. Also, all models for DZP, TZP, and NDP metabolism all gave K_{m2}/K_{m1} ratios of ∼0.5. This allowed us to construct model 5, for which the fitted results are shown in Table 7. In this model, P3 formation from EP2 and ESP2 is four times that from EP1 and ESP1. K_m values for the formation of ESP1 and ESP2 are half that for EP1 and EP2. With this model, all parameters could be optimized with the exception of K_{m3}, which had to be optimized and fixed.

For MDZ, the mean clinical clearance value was 461 ml/min (obtained from drugbank.ca), whereas the predicted clearance from ESS model (model 2b) = 677 ml/min versus predicted from MM (model 1a) = 753 ml/min. Compared with the mean clinical clearance value (obtained from drugbank.ca) for DZP (25 ml/min), the predicted clearance values were as follows. For DZP, predicted clearance from ESS model (model 5) = 47 ml/min versus predicted from MM (model 1a) = 362 ml/min. Clearance

TABLE 4

Scheme and kinetic parameters for ticlopidine metabolism with a two-substrate model

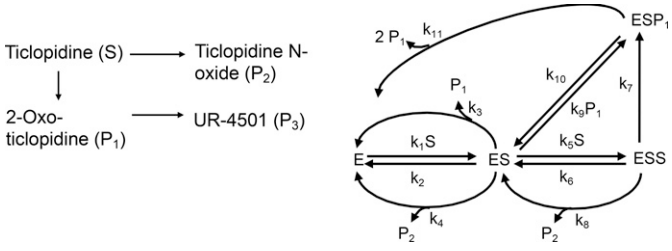

Kinetic Parameters	ESSP1P2 ODE Simultaneous Product Fit		
2-Oxo-TCP		**TCP *N*-Oxide**	
K_{m1} (μM) = $(k_2+k_3+k_4)/k_1$	38.9 (fixed)	K_{m1} (μM) = $k_1/(k_2+k_3+k_4)$	38.9 (fixed)
k_{cat1} (min^{-1}) = k_3	2.8 (0.4)	k_{cat1} (min^{-1}) = k_4	3.1 (0.4)
k_{cat1}/K_{m1} ($ml\ min^{-1}nmol^{-1}$)	0.073 (fixed)	k_{cat1}/K_{m1} ($ml\ min^{-1}nmol^{-1}$)	0.079 (fixed)
K_{m2} (μM) = $(k_6+k_7+k_8)/k_5$	707 (559)	K_{m2} (μM) $k_5/(k_6+k_7+k_8)$	707 (559)
k_{cat2}(min^{-1}) = k_7	3.5 (2.0)	k_{cat2} (min^{-1}) = k_8	20 (10)
K_{m3} (μM) = $(k_{10}+k_{11})/k_9$	0.32 (fixed)		
k_{cat3} (min^{-1}) = k_{11}	59 (14)	AICc	−338.5

ESSP1P2, enzyme-substrate-substrate complex scheme with two products formed.

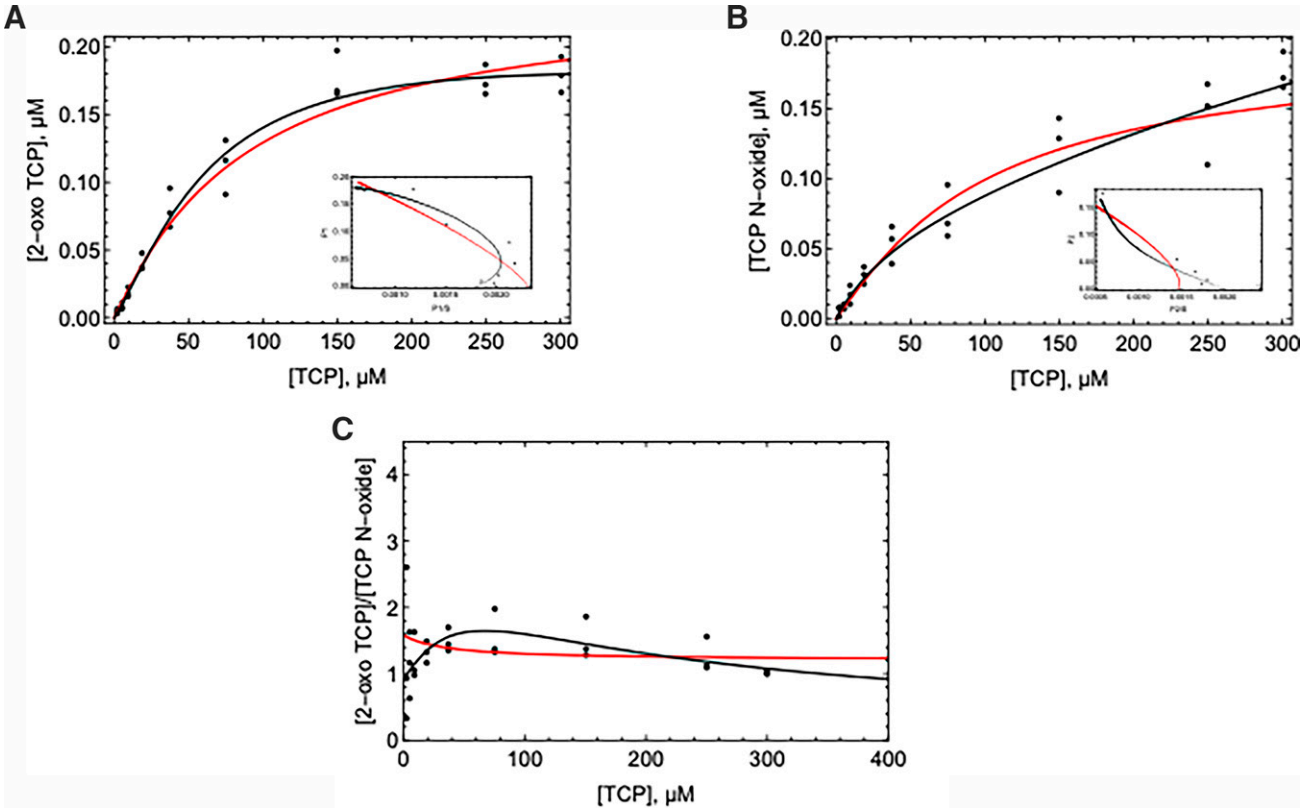

Fig. 4. Kinetic plots of ticlopidine metabolism by CYP3A4 (n = 3) for the formation of (A) 2-oxo-ticlopidine and (B) ticlopidine *N*-oxide and (C) ratio of 2-oxo-ticlopidine to ticlopidine *N*-oxide. Insets represent EH plots with mean data. The solid lines represent the fit with model 2b (red) and model 3 (black).

predictions for TCP were not attempted because of contribution of several enzymes besides CYP3A4 toward its systemic clearance.

Discussion

In part 1 we modeled P450 metabolism using simulated datasets that included sigmoidal saturation kinetics and sequential metabolism. In this paper we generated datasets and developed kinetic models for three substrates that show both non–Michaelis-Menten kinetics and sequential metabolism. For two of the substrates, MDZ and TCP, we had primary metabolites available but no standards for secondary metabolites. This is similar to the situation during lead optimization when clearances are being predicted, but the fate of the primary metabolites is unknown, or secondary metabolite standards are not available. For DZP, we have very rich data, including the formation of primary and secondary metabolites from parent and metabolism data for the secondary metabolites.

Model 1a and b (MM kinetics) were fit to all datasets, and in most cases, better fits were obtained with two-substrate models (Supplemental Table S1; Tables 2–7). For 4-OH-MDZ and TCP *N*-oxide, similar AICc values were obtained for MM and model2a, but the EH plots show that the kinetics are clearly biphasic (Fig. 3B and 4B). For all substrates, differences in calculated k_{cat}/K_m values varied between 1.25-fold for TCP *N*-oxide and 14-fold for TZP.

Comparing the ESS rate equation models to the ESS ODE models, model fits for MDZ and DZP are statistically identical. For TCP, the rate equation does not converge to meaningful estimates for the TCP *N*-oxide data, whereas the ODE model does. Rate equations are derived from ODE models and should provide identical results. Differences will occur when the assumptions used in the derivation (initial rates and steady state) do not hold.

Multisubstrate binding kinetics for midazolam is well known, and a recent report provides evidence for the binding regions for two midazolam molecules (Denisov et al., 2021). For the models in this report, it is not necessary to identify which substrate molecule is metabolized to which product. Observed results, including changing product ratios, require appropriate formation rates of 1′-OH-MDZ and 4-OH-MDZ from ES and ESS complexes. For MDZ metabolism, it was necessary to fix one parameter because of covariance when P1 and P2 were modeled separately. When modeled together, all parameters could be solved for, with P1 formation showing substrate inhibition and P2 formation showing biphasic saturation kinetics. Consequently, k_{cat1}/K_1 can be well defined for clearance prediction efforts. For the biphasic saturation curve, the second binding site is adequately saturated such that K_{m2} and k_{cat2} can be defined (Table 2). There do appear to be nonrandom residuals (Fig. 3A), suggesting further complexities are not modeled. Since both 1′-OH-MDZ and 4-OH-MDZ are further metabolized, this could impact the saturation curves. In the absence of the secondary metabolite standard, we were unable to find a statistically better model than model 2a.

Classic cooperativity (e.g., the Hill equation) results in sigmoidal kinetics due to cooperative binding of the second substrate once the first substrate binds to the enzyme. This can be modeled as an ESS model. The Hill equation is especially useful when the mechanism of enzyme/receptor-substrate cooperativity is known. In drug metabolism, parameterization of sigmoidal kinetics can be problematic in two ways: first, since both $K_{m1} > K_{m2}$ and $k_{cat2} > k_{cat1}$ can cause sigmoidicity, these parameters are covariant when error is present. Second, very low k_{cat1} values can result in k_{cat}/K_m values that are substrate-concentration dependent at low substrate concentrations (Korzekwa, 2014). Sigmoidal kinetics was observed in the metabolism of both TCP and DZP (discussed below). Although 2-oxo-TCP shows sigmoidal kinetics based on the diagnostic hooked EH plot, none of the model fits conform to classic cooperativity (Tables 3 and 4).

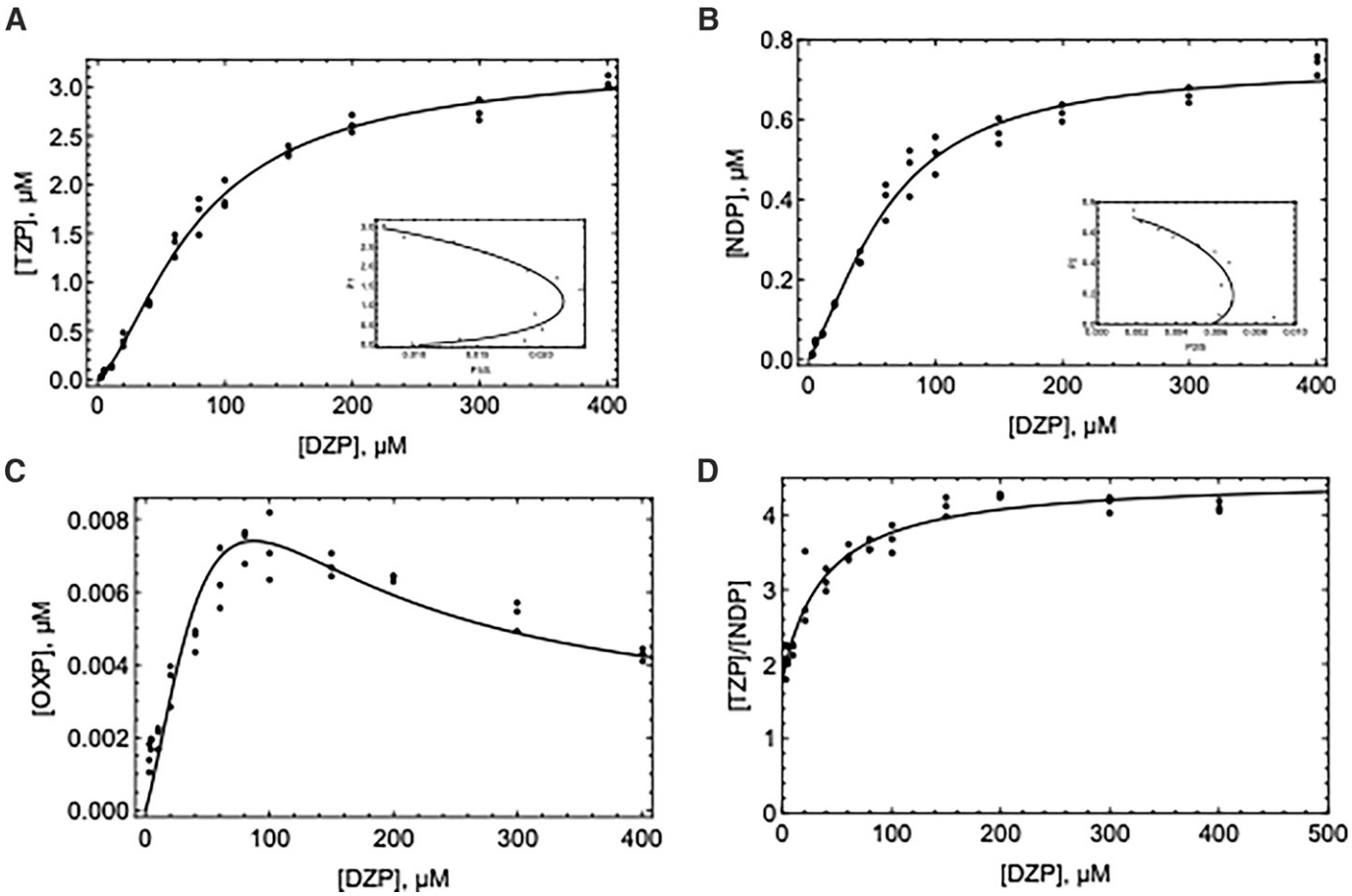

Fig. 5. Kinetic plots of diazepam metabolism by CYP3A4 (n = 3) for the formation of (A) temazepam, (B) nordiazepam, (C) oxazepam, and (D) ratio of temazepam and nordiazepam. Insets represent EH plots with mean data. The solid lines represent the fit with model 5.

Fits to models 2a and 2b clearly do not reproduce the EH plots or the metabolite ratio plot (red lines in Fig. 4). Since we know that P1 is further metabolized to P3, a number of other models for sequential metabolism were tested. Models with rapid P1 release failed to improve the predictions. The observed data could be modeled best by including an explicit ESP1 complex. In the absence of P3 data, any ratio of P1 conversion to

TABLE 5

Scheme and kinetic parameters for diazepam metabolism with a two-substrate model

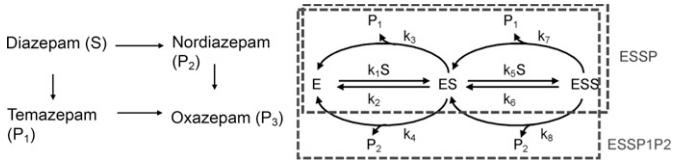

Kinetic Parameters	ESS Rate Equation	ESSP ODE	ESSP1P2 ODE
	TZP		**TZP**
K_{m1} (μM) = $(k_2+k_3+k_4)/k_1$	112 (70)	110 (68)	92 (37)
k_{cat1} (min^{-1}) = k_3	20 (15)	20 (15)	16 (9)
k_{cat1}/K_{m1} ($ml\ min^{-1}nmol^{-1}$)	0.18 (0.18)	0.18 (0.18)	0.18 (12)
K_{m2} (μM) = $(k_6+k_7+k_8)/k_5$	47 (16)	47 (16)	51 (10)
k_{cat2} (min^{-1}) = k_7	54 (3)	54.4 (3.4)	93 (37)
AICc	−78.9	−78.9	
	NDP		**NDP**
K_{m1} (μM) = $(k_2+k_3+k_4)/k_1$	65 (50)	64 (51)	92 (37)
k_{cat1} (min^{-1}) = k_4	6.1 (5.6)	6 (6)	8.9 (3.6)
k_{cat1}/K_{m1} ($ml\ min^{-1}nmol^{-1}$)	0.09 (0.11)	0.09 (0.11)	0.10 (0.06)
K_{m2} (μM) $(k_6+k_7+k_8)/k_5$	58 (12)	58 (12)	51 (10)
k_{cat2} (min^{-1}) = k_8	12.9 (1.0)	12.8 (1.0)	12.3 (0.8)
AICc	−155.7	−155.7	−558.5

ESSP, enzyme-substrate-substrate complex scheme with single product formation; ESSP1P2, enzyme-substrate-substrate complex scheme with two products formed.

TABLE 6

Scheme and kinetic parameters for diazepam metabolism with a two-substrate model and simultaneous fitting to P1, P2, and P3

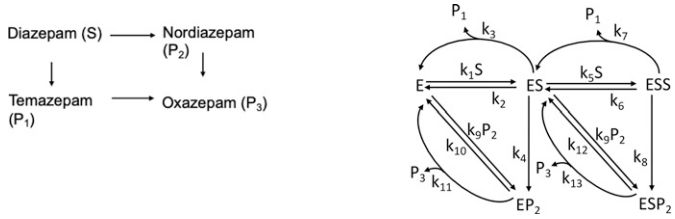

ESSP1P2P3 ODE Simultaneous Product Fit					
TZP		**NDP**		**OXP**	
K_{m1} (μM) = $(k_2+k_3+k_4)/k_1$	92 (fixed)	K_{m1} (μM) = $(k_2+k_3+k_4)/k_1$	92 (fixed)	K_{m3} (μM) = $(k_{10}+k_{11})/k_9$	50 (fixed)
k_{cat1}(min^{-1}) = k_3	15.9 (1.8)	k_{cat1} (min^{-1}) = k_4	9.0 (0.7)	k_{cat3} (min^{-1}) = k_{11}	10 (4)
k_{cat1}/K_{m1} (ml $min^{-1}nmol^{-1}$)	0.17 (fixed)	k_{cat1}/K_{m1} (ml $min^{-1}nmol^{-1}$)	0.098 (fixed)	k_{cat3}/K_{m3} (ml $min^{-1}nmol^{-1}$)	0.20(fixed)
K_{m2} (μM) = $(k_6+k_7+k_8)/k_5$	50 (4)	K_{m2} (μM) = $(k_6+k_7+k_8)/k_5$	50 (4)	K_{m4} (μM) = $(k_{12}+k_{13})/k_9$	25 (fixed)
k_{cat2} (min^{-1}) = k_7	56.5 (1.0)	k_{cat2} (min^{-1}) = k_8	12.6 (0.4)	k_{cat4} (min^{-1}) = k_{13}	3.6 (1.4)
AICc = −564.0					

ESSP1P2P3, enzyme-substrate-substrate complex scheme with three products formed.

either P1 or P3 provides identical fits. Therefore, the simplest model (no P3 formation) is presented in Table 4.

All primary and secondary metabolites of DZP show sigmoidal saturation kinetics. This complexity can be modeled only with the availability of rich datasets. For DZP, we generated data of S being metabolized to P1, P2, and sequentially P3 as well as P1 and P2 each metabolized to P3. Even with this dataset, two assumptions were necessary: 1) The affinity of the ESP complexes were twice those for the EP complexes, and 2) the ratio of P3 formation from P1 versus from P2 was fixed at 4. The first assumption is based on the observation that K_m values for ESS complexes are approximately half those for ES complexes (Tables 5–7). The second assumption is based on the k_{cat1}/K_{m1} values for conversion of P1 and P2 to P3 (Supplemental Fig. S2). It is necessary to fix either k_{cat3} or K_{m3} for any model with sequential metabolism since V_{max}/K_m conditions will apply (Tables 4 for TCP and Tables 6 and 7 for DZP).

The clinical relevance of these studies is apparent for drugs with atypical kinetics and for drugs with metabolites that are further converted to either active or toxic metabolites. Accurate determination of k_{cat}/K_m is essential for in vivo clearance predictions. Use of the Michaelis-Menten model can result in highly inaccurate kinetic parameters (Supplemental Table S1). Parameters from the MM model resulted in poor predictions of in vivo clearance of both MDZ and DZP. On the other hand, clearance was better predicted with ESS model parameters (within 2-fold for both drugs). The importance of accurately modeling sequential metabolism for prodrugs and drugs with active metabolites cannot be overstated. These methods can also be used for other sequential metabolic pathways, including conjugation reactions that are often reversible and result in enterohepatic recirculation in vivo.

It should also be noted that sequential metabolism within a closed environment of an in vitro incubation may not accurately represent sequential metabolism in an open in vivo system, such as a drug traversing a liver sinusoid. Further research in this area is necessary. Finally, it is clear that modeling complex kinetics (and simple kinetics as well) can be easily performed using ODEs and numerical analyses.

TABLE 7

Scheme and kinetic parameters for diazepam metabolism with a two-substrate model and simultaneous fitting to P1, P2, and P3 using metabolite incubation data

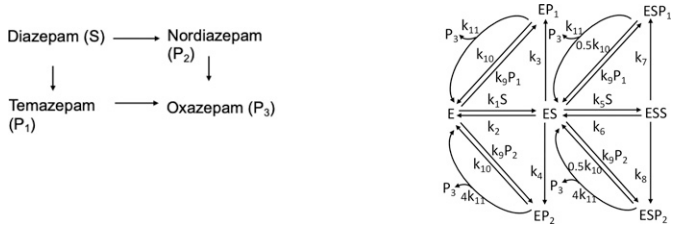

ESSP1P2P3 ODE Simultaneous Product Fit					
TZP		**NDP**		**OXP**	
K_{m1} (μM) = $(k_2+k_3+k_4)/k_1$	94 (30)	K_{m1} (μM) = $(k_2+k_3+k_4)/k_1$	94 (30)	K_{m3} (μM) = $(k_{10}+k_{11})/k_9$	167 (fixed)
k_{cat1}(min^{-1}) = k_3	17 (7)	k_{cat1} (min^{-1}) = k_4	9.3 (3.0)	k_{cat3} (min^{-1}) = k_{11}	18 (7)
k_{cat1}/K_{m1} (ml $min^{-1}nmol^{-1}$)	0.18 (0.09)	k_{cat1}/K_{m1} (ml $min^{-1}nmol^{-1}$)	0.1 (0.05)	k_{cat3}/K_{m3}(ml $min^{-1}nmol^{-1}$)	0.11 (fixed)
K_{m2} (μM) = $(k_6+k_7+k_8)/k_5$	50 (8)	K_{m2} (μM) = $(k_6+k_7+k_8)/k_5$	50 (8)		
k_{cat2} (min^{-1}) = k_7	55.6 (1.8)	k_{cat2} (min^{-1}) = k_8	12.4 (0.6)		
AICc = −561.9					

ESSP1P2P3, enzyme-substrate-substrate complex scheme with three products formed.

Authorship Contributions

Participated in research design: Paragas, Wang, Korzekwa.

Conducted experiments: Paragas, Wang.

Performed data analysis: Paragas, Wang, Korzekwa, Nagar.

Wrote or contributed to the writing of the manuscript: Paragas, Wang, Korzekwa, Nagar.

References

Akaike H (1974) A new look at the statistical model identification. *IEEE Trans Automat Contr* **19**:716–723.

Barnaba C, Yadav J, Nagar S, Korzekwa K, and Jones JP (2016) Mechanism-based inhibition of CYP3A4 by podophyllotoxin: aging of an intermediate is important for in vitro/in vivo correlations. *Mol Pharm* **13**:2833–2843.

Caccia S and Garattini S (1990) Formation of active metabolites of psychotropic drugs. An updated review of their significance. *Clin Pharmacokinet* **18**:434–459.

Cameron MD, Wen B, Allen KE, Roberts AG, Schuman JT, Campbell AP, Kunze KL, and Nelson SD (2005) Cooperative binding of midazolam with testosterone and alpha-naphthoflavone within the CYP3A4 active site: a NMR T1 paramagnetic relaxation study. *Biochemistry* **44**:14143–14151.

Denisov IG, Grinkova YV, Camp T, McLean MA, and Sligar SG (2021) Midazolam as a probe for drug-drug interactions mediated by CYP3A4: homotropic allosteric mechanism of site-specific hydroxylation. *Biochemistry* **60**:1670–1681.

Di L (2017) Reaction phenotyping to assess victim drug-drug interaction risks. *Expert Opin Drug Discov* **12**:1105–1115.

Ekroos M and Sjögren T (2006) Structural basis for ligand promiscuity in cytochrome P450 3A4. *Proc Natl Acad Sci USA* **103**:13682–13687.

Farid NA, Kurihara A, and Wrighton SA (2010) Metabolism and disposition of the thienopyridine antiplatelet drugs ticlopidine, clopidogrel, and prasugrel in humans. *J Clin Pharmacol* **50**:126–142.

Garattini S (1985) Active drug metabolites. An overview of their relevance in clinical pharmacokinetics. *Clin Pharmacokinet* **10**:216–227.

He YA, Roussel F, and Halpert JR (2003) Analysis of homotropic and heterotropic cooperativity of diazepam oxidation by CYP3A4 using site-directed mutagenesis and kinetic modeling. *Arch Biochem Biophys* **409**:92–101.

Hijazi Y and Boulieu R (2002) Protein binding of ketamine and its active metabolites to human serum. *Eur J Clin Pharmacol* **58**:37–40.

Kapelyukh Y, Paine MJI, Maréchal J-D, Sutcliffe MJ, Wolf CR, and Roberts GCK (2008) Multiple substrate binding by cytochrome P450 3A4: estimation of the number of bound substrate molecules. *Drug Metab Dispos* **36**:2136–2144.

Kawato Y, Aonuma M, Hirota Y, Kuga H, and Sato K (1991) Intracellular roles of SN-38, a metabolite of the camptothecin derivative CPT-11, in the antitumor effect of CPT-11. *Cancer Res* **51**:4187–4191.

Korzekwa K (2014) Enzyme kinetics of oxidative metabolism: cytochromes P450. *Methods Mol Biol* **1113**:149–166.

Korzekwa KR, Krishnamachary N, Shou M, Ogai A, Parise RA, Rettie AE, Gonzalez FJ, and Tracy TS (1998) Evaluation of atypical cytochrome P450 kinetics with two-substrate models: evidence that multiple substrates can simultaneously bind to cytochrome P450 active sites. *Biochemistry* **37**:4137–4147.

Li H and Poulos TL (2004) Crystallization of cytochromes P450 and substrate-enzyme interactions. *Curr Top Med Chem* **4**:1789–1802.

Nguyen HQ, Kimoto E, Callegari E, and Obach RS (2016) Mechanistic modeling to predict midazolam metabolite exposure from in vitro data. *Drug Metab Dispos* **44**:781–791.

Obach RS (2011) Predicting clearance in humans from in vitro data. *Curr Top Med Chem* **11**:334–339.

Obach RS (2013) Pharmacologically active drug metabolites: impact on drug discovery and pharmacotherapy. *Pharmacol Rev* **65**:578–640.

Rouini MR, Ardakani YH, Moghaddam KA, and Solatani F (2008) An improved HPLC method for rapid quantitation of diazepam and its major metabolites in human plasma. *Talanta* **75**:671–676.

Schoch GA, Yano JK, Sansen S, Dansette PM, Stout CD, and Johnson EF (2008) Determinants of cytochrome P450 2C8 substrate binding: Structures of complexes with montelukast, troglitazone, felodipine, and 9-cis-retinoic acid **283**:17227-17237.

Sevrioukova IF and Poulos TL (2017) Structural basis for regiospecific midazolam oxidation by human cytochrome P450 3A4. *Proc Natl Acad Sci USA* **114**:486–491.

Shah MB, Wilderman PR, Pascual J, Zhang Q, Stout CD, and Halpert JR (2012) Conformational adaptation of human cytochrome P450 2B6 and rabbit cytochrome P450 2B4 revealed upon binding multiple amlodipine molecules. *Biochemistry* **51**:7225–7238.

Vieira MLT, Kirby B, Ragueneau-Majlessi I, Galetin A, Chien JYL, Einolf HJ, Fahmi OA, Fischer V, Fretland A, Grime K, et al. (2014) Evaluation of various static in vitro-in vivo extrapolation models for risk assessment of the CYP3A inhibition potential of an investigational drug. *Clin Pharmacol Ther* **95**:189–198.

Wienkers LC and Rock B (2014) Multienzyme kinetics and sequential metabolism. *Methods Mol Biol* **1113**:93–118.

Yadav J, Korzekwa K, and Nagar S (2018) Improved predictions of drug-drug interactions mediated by time-dependent inhibition of CYP3A. *Mol Pharm* **15**:1979–1995.

Yadav J, Paragas E, Korzekwa K, and Nagar S (2020) Time-dependent enzyme inactivation: numerical analyses of in vitro data and prediction of drug-drug interactions. *Pharmacol Ther* **206**:107449.

Yoneda K, Iwamura R, Kishi H, Mizukami Y, Mogami K, and Kobayashi S (2004) Identification of the active metabolite of ticlopidine from rat in vitro metabolites. *Br J Pharmacol* **142**:551–557.

Zhang Z-Y and Wong YN (2005) Enzyme kinetics for clinically relevant CYP inhibition. *Curr Drug Metab* **6**:241–257.

Address correspondence to: Dr. Swati Nagar, 3307 N. Broad St., Philadelphia, PA 19140. E-mail: swati.nagar@temple.edu